Institute of
Applied Mechanics
Institut für Baumechanik

Graz University of Technology

Preprint Series

Institute of Applied Mechanics

Graz University of Technology

Preprint No 2/2009

An Extendable Poroelastic Plate Formulation in Dynamics

Loris Nagler
&
Martin Schanz
Institute of Applied Mechanics, Graz University of Technology

Published in: *Archive of Applied Mechanics*, 80(10),
1177-1195, 2010

Latest revision: September 01,

Abstract

A strategy is presented which allows deriving poroelastic plate formulations of any desired level of approximation. Starting point are the governing three-dimensional (3d) equations of poroelasticity in frequency domain developed by Biot. In order to reduce the dimension of the problem from 3d to 2d, all unknown quantities are approximated by series expansions in thickness direction. This avoids the need for any engineering assumptions. The reduction of the dimension can then be achieved by an integration over the thickness. After truncating the series, a special plate formulation is retrieved. Results are presented for a square, clamped plate which show excellent agreement with the solution of the 3d equations and a considerable saving in computation time.

1 Introduction

Noise mitigation is a subject of large interest in different fields of engineering, as in the building industry, car or aeronautical industry. The main concern is basically the reduction of the sound pressure between the source and the receptor, hence, to absorb the energy of the sound waves using damping structures. When soundproofing the interior of a room or a car, such damping structures may be found in poroelastic plate-like elements. A first step in the attempt to develop a mathematical model to simulate sound insulation consists in examining the dynamic behavior of such porous structures.

The first self-consistent theory of wave propagation in poroelastic solids has been developed by Biot [2, 4]. He also dealt with the anisotropic case [3] and with poroviscoelasticity [5]. Although it has been shown that Biot's theory is not fully consistent within the framework of thermodynamics [22], it enjoys wide popularity and has proven itself in many engineering fields. In the present work, Biot's theory is used to model the poroelastic behavior.

Poroelastic plate formulations can already be found in the literature. A plate formulation based on the same assumptions as for an elastic Kirchhoff plate has been presented by Taber [20] for the quasi-static case. A Kirchhoff plate theory for the poroelastodynamic equations has been presented by Theodorakoupolos and Beskos [21]. Applications of this formulation with further simplifications, e.g., for incompressible constituents, can be found in [15]. Taber, as well as Theodorakoupolos and Beskos, assumed the in-plane flux to be negligible. In contrast to those works, Cederbaum et al. [8] investigated various poroelastic structures for which the in-plane flux is viable, while it is negligible in the perpendicular direction.

It is well known that the Kirchhoff assumptions are only valid for thin plates. In view of the problems of sound mitigation, the use of thin plates may be too restrictive. But even the extension to higher order theories, e.g., Mindlin or Reissner plate theory, does not answer the question whether the kinematical assumptions made for the displacements can be transferred to the pore pressure as well.

The possibility of bypassing the problem of making any kind of such assumptions can be found in the systematic way to develop plate theories based on series expansions for the degrees of freedom (dofs) in the thickness direction. For the linear elastic case such an approach has already been used by Mindlin [17]. Works using this kind of series expansions have also been published by Preusser [18] or more recently by Kienzler [12, 13]. The main difference therein is the different way in truncating the series expansions. Especially Kienzler [12] showed how to obtain the classical plate equations by using this method.

Here, using the method of series expansions, a general framework for the development of assumption-free poroelastic plate theories is presented, easily extendible to any needed order. One special plate formulation is then deduced from this framework. The so obtained system is solved numerically using the finite element method (FEM). The results are validated by comparing them to the solution of the three-dimensional (3d) Biot model.

In the following, all equations are stated in the frequency domain under the assumption that all quantities have a time-harmonic behavior (x_i being the spatial, and t the time coordinate), i.e.,

$$\tilde{\chi}(x_i,t) = \chi(x_i)e^{\mathrm{i}\omega t}$$

with the imaginary unit i and the angular frequency ω (χ stands for any time-dependent quantity

in the system). Further, index-notation is used assuming an orthonormal Cartesian basis $\{\mathbf{e}_i\}$. Herein, a summation on repeated indices is imposed, a comma $()_{,i}$ denotes the spatial derivative and, as usual, the Kronecker delta is denoted by δ_{ij}. Throughout the paper, latin indices i, j, k take on the values $1, 2, 3$ whereas greek indices α, β, γ take on the values $1, 2$.

2 Biot's theory

Biot's theory of poroelasticity leads to a system of seven partial differential equations in time domain determining the solid and the fluid displacement fields u_i and u_i^f as well as the pore pressure p. The system, however, can be modified such to consider only the four degrees of freedom u_i and p [1]. This latter case is only possible in Laplace domain or, as a special case, in the frequency domain. In this work, this so called u_i-p formulation is used.

A saturated poroelastic continuum is composed of a solid skeleton with volume V_s and a system of fluid-filled interconnected pores with volume V_f. The porosity ϕ is defined as the ratio of the fluid volume to the total volume, $\phi = {}^{V_f}/_{V}$ with $V = V_S + V_f$. Sealed pores, whether saturated or not, are taken to be part of the solid phase and, hence, do not affect the porosity ϕ.

Using the total stress σ_{ij} and the variation of fluid per unit volume ζ [2], the constitutive relations have the form

$$\sigma_{ij} = 2\mu\varepsilon_{ij} + \lambda\varepsilon_{kk}\delta_{ij} - \alpha p\delta_{ij} \tag{1a}$$

$$\zeta = \alpha\varepsilon_{kk} + \frac{\phi^2}{R}\, p\,. \tag{1b}$$

In (1), ε_{ij} denotes the components of the solid strain tensor and ε_{kk} its trace. The material is characterized by four parameters, which are the two Lamé parameters μ and λ describing the solid skeleton and the two parameter R and α describing the coupling between the solid and the fluid. The strain-displacement relation between ε_{ij} and u_i is chosen to be linear

$$\varepsilon_{ij} = \frac{1}{2}(u_{i,j} + u_{j,i})\,. \tag{2}$$

The quantity ζ is defined by the continuity equation

$$\mathrm{i}\omega\zeta + q_{i,i} = 0\,, \tag{3}$$

with $q_{i,i}$ denoting the divergence of the fluid flux. The flux q_i is defined as a quantity proportional to the relative velocity between the fluid and the solid, namely

$$q_i = \phi\,\mathrm{i}\omega(u_i^f - u_i)\,. \tag{4}$$

The fluid flow is modeled using a dynamic version of Darcy's law [19]

$$q_i = -\kappa\left(p_{,i} - \omega^2\frac{\rho^a - \phi\rho^f}{\phi}(u_i^f - u_i) - \omega^2\rho^f u_i - f_i^f\right), \tag{5}$$

where κ denotes the permeability which takes into account the fluid viscosity and ρ^f and f^f denote the fluid density and its volume force, respectively. The apparent mass density ρ^a has

been introduced by Biot [4] and can be written as $\rho^a = C\phi\rho^f$. For a lower frequency range, C can be assumed to take the value $C = 0.66$, whereas for higer frequency ranges, a dependency of C on the frequency has been proposed in [6, 11]. By combining (4) and (5) q_i can be expressed as a function of (u_i, p)

$$q_i = -\frac{\beta}{i\omega\rho^f}(-p_{,i} + \omega^2\rho^f u_i + f_i^f)\,. \tag{6}$$

The dimensionless factor β is defined as

$$\beta := \frac{\omega^2\rho^f\phi^2\kappa}{i\omega\phi^2 - \kappa\omega^2(\rho^a + \phi\rho^f)}\,.$$

The balance of momentum of the mixture is written as

$$\sigma_{ij,j} + f_i + \omega^2\rho u_i = \beta\left(p_{,i} - f_i^f - \omega^2\rho^f u_i\right) \tag{7}$$

with $\rho = (1-\phi)\,\rho^s + \phi\,\rho^f$ being the bulk density and $f_i = (1-\phi)\,f_i^s + \phi\,f_i^f$ the bulk body force. The full set of differential equations governing the dynamic behavior of a poroelastic continuum is obtained by combining the constitutive equation (1a) with the kinematic relation (2) and the balance equation (7) and by combining the constitutive equation (1b) with the kinematic relation (2) and the continuity equation (3) and, further, by eliminating q_i using (6). The final set reads

$$\mu u_{i,jj} + (\lambda+\mu)\,u_{j,ij} - (\alpha+\beta)\,p_{,i} + \omega^2(\rho + \beta\rho^f)\,u_i = -(f_i + \beta\,f_i^f) \tag{8a}$$

$$\frac{\beta}{i\omega\rho_f}\,p_{,jj} + i\omega\frac{\phi^2}{R}\,p + i\omega(\alpha+\beta)\,u_{j,j} = \frac{\beta}{i\omega\rho_f}\,f_{j,j}^f\,. \tag{8b}$$

If the porosity ϕ is assumed to be zero, the system (8) reduces to the wave equation of linear elasticity.

Aiming on a finite element formulation, the system (8) can be written in a variational form. Therefore, both equations in (8) are multiplied by the variations $\bar{u}_i$ and $\bar{p}$, respectively, and integrated over the whole domain $\Omega \subset \mathbb{R}^3$. An integration by parts yields

$$\int_\Omega [\sigma_{ij}\,\bar{u}_{i,j} - \zeta\,\bar{p}]\,d\Omega + \int_\Omega \left[\sigma_{ij,j}\,\bar{u}_i + \frac{1}{i\omega}q_i\,\bar{p}_{,i}\right] d\Omega - \int_{\Gamma_t}\left[t_i\,\bar{u}_i + \frac{1}{i\omega}\,q_n\,\bar{p}\right] d\Gamma_t = 0\,. \tag{9}$$

The quantities on Γ_t are the surface stresses $t_i = \sigma_{ij}\,n_i$ and the surface flux $q_n = q_i\,n_i$, n_i being the components of the outward normal vector. The boundary Γ_t denotes the Neumann boundary, i.e., the part of the boundary where t_i and/or q_n are prescribed.

3 The two-dimensional work equation

Usually, plate equations are understood as two-dimensional equations, i.e., all quantities appearing in such equations are functions of two independent space coordinates only. In order to justify the description of a three-dimensional structure in two dimensions only, its geometry has to be "plate-like". The thickness h of the plate in x_3-direction is assumed to be much smaller

than its extensions in the (x_1,x_2)-plane. The mid-surface divides the plate into a lower and an upper part such that $x_3 \in [-h/2,+h/2]$ holds. Figure 1 shows the original three-dimensional plate geometry and its two-dimensional representation depicted by the gray area A with the boundary C. The normal and tangential vectors $\mathbf{n}$ and $\mathbf{s}$ on C only have nonzero components in x_1- and x_2-direction.

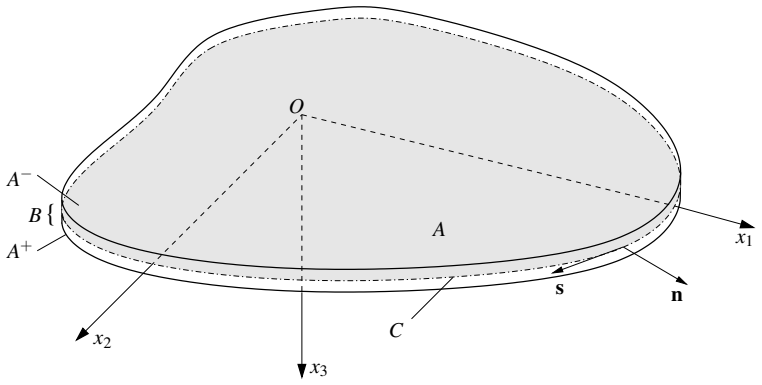

Figure 1: The geometry and definitions of the plate

In 2d, the plate is described solely by its mid-surface. This means that ideally all information contained in the thickness has to be mapped onto the mid-surface. Hence, a 2d work equation is obtained by integrating (9) over the thickness. Obviously, an integration demands the knowledge of the function to be integrated, especially its dependence on the variable of integration. Some functions as the material parameters, the porosity and the body forces are assumed to be constant throughout the whole plate domain. The main problem lies in integrating the unknown functions u_i and p. For elastic plates, the usual approach is to introduce some assumptions regarding the distribution of u_i, σ_{ij} and/or ε_{ij} over the thickness. In the present case, however, it is questionable whether the same assumptions can be extended to the pore pressure p.

An alternative approach which gets along without such assumptions consists in replacing the unknown functions by power series expansions in thickness direction. Following this idea, the power series

$$u_i(x_1,x_2,x_3) = \sum_{k=0}^{\infty} \overset{k}{u}_i(x_1,x_2)\, x_3^k \qquad p(x_1,x_2,x_3) = \sum_{k=0}^{\infty} \overset{k}{p}(x_1,x_2)\, x_3^k \tag{10a}$$

$$\bar{u}_i(x_1,x_2,x_3) = \sum_{\ell=0}^{\infty} \overset{\ell}{\bar{u}}_i(x_1,x_2)\, x_3^\ell \qquad \bar{p}(x_1,x_2,x_3) = \sum_{\ell=0}^{\infty} \overset{\ell}{\bar{p}}(x_1,x_2)\, x_3^\ell \tag{10b}$$

are introduced for the unknown functions and their variations. Since a function is always multiplied by its respective variation, the series (10a) and (10b) are assigned to different summation indices, i.e., k and ℓ, respectively. In (10), with the power series the dependency of u_i, p, $\bar{u}_i$, and $\bar{p}$ on x_3 is now given explicitly. This, in turn, introduces an infinite number of coefficients of order k,ℓ. Those, however, are now functions of the in-plane coordinates only and the needed integration over the thickness of the three-dimensional work equation in (9) can be performed.

3.1 The domain integral

Before doing so, the two domain integrals in (9) are merged and, for convenience, ζ is replaced using the continuity equation ! (3). This yields

$$\int_\Omega [\sigma_{ij}\,\bar{u}_{i,j} - \zeta\,\bar{p}]\,\mathrm{d}\Omega + \int_\Omega \left[\sigma_{ij,j}\,\bar{u}_i + \frac{1}{\mathrm{i}\omega} q_i\,\bar{p}_{,i}\right]\mathrm{d}\Omega = \int_\Omega \left[\sigma_{ij}\,\bar{u}_{i,j} + \sigma_{ij,j}\,\bar{u}_i + \frac{1}{\mathrm{i}\omega}\left(q_{i,i}\,\bar{p} + q_i\,\bar{p}_{,i}\right)\right]\mathrm{d}\Omega\,. \tag{11}$$

Furthermore, so-called resultants are introduced which, partly, can be assigned to a distinct physical meaning. Those are defined as

$$\overset{\ell}{S}_{ij} = \int_h \left[\sigma_{ij}\,x_3^\ell\right]\mathrm{d}x_3 \qquad \overset{\ell}{Q}_i = \int_h \left[q_i\,x_3^\ell\right]\mathrm{d}x_3 \tag{12a}$$

$$\overset{\ell}{T}_i = \int_h \left[\sigma_{ij,j}\,x_3^\ell\right]\mathrm{d}x_3 \qquad \overset{\ell}{P} = \int_h \left[q_{i,i}\,x_3^\ell\right]\mathrm{d}x_3\,. \tag{12b}$$

The resultants (12a) are stress and flux resultants, respectively, whereas the resultants (12b) are mainly introduced for convenience without a distinct physical interpretation.

It is required to separate the tensor components into the out-of-plane and the in-plane components. It is obvious that it must be distinguished between a differentiation with respect to the in-plane coordinates x_α and the thickness coordinate x_3. The gradient operator applied on (10a) for example gives

$$\mathrm{grad}\,u_i = u_{i,j} = \sum_{k=0}^{\infty} \begin{bmatrix} \overset{k}{u}_{\alpha,\beta}\,x_3^k & k\,\overset{k}{u}_\alpha\,x_3^{k-1} \\ \overset{k}{u}_{3,\beta}\,x_3^k & k\,\overset{k}{u}_3\,x_3^{k-1} \end{bmatrix} \qquad \mathrm{grad}\,p = p_{,i} = \sum_{k=0}^{\infty} \begin{bmatrix} \overset{k}{p}_{,\alpha}\,x_3^k \\ k\,\overset{k}{p}\,x_3^{k-1} \end{bmatrix}.$$

By inserting the series expansions (10b) into (11) for the variations $\bar{u}_i$ and $\bar{p}$ only, yields

$$\begin{aligned} &\int_\Omega \left[\sigma_{ij}\,\bar{u}_{i,j} + \sigma_{ij,j}\,\bar{u}_j + \frac{1}{\mathrm{i}\omega}\left(q_{i,i}\,\bar{p} + q_i\,\bar{p}_{,i}\right)\right]\mathrm{d}\Omega = \\ &\int_\Omega \sum_{\ell=0}^{\infty} \Bigg[\left(\sigma_{i\alpha}\,x_3^\ell\right)\overset{\ell}{\bar{u}}_{i,\alpha} + \ell\left(\sigma_{i3}\,x_3^{\ell-1}\right)\overset{\ell}{\bar{u}}_i + \left(\sigma_{ij,j}\,x_3^\ell\right)\overset{\ell}{\bar{u}}_i + \\ &\qquad \frac{1}{\mathrm{i}\omega}\left(\left(q_\alpha\,x_3^\ell\right)\overset{\ell}{\bar{p}}_{,\alpha} + \ell\left(q_3\,x_3^{\ell-1}\right)\overset{\ell}{\bar{p}} + \left(q_{i,i}\,x_3^\ell\right)\overset{\ell}{\bar{p}}\right)\Bigg]\mathrm{d}\Omega\,. \end{aligned} \tag{13}$$

The integral over the domain Ω can be split according to $\int_\Omega \mathrm{d}\Omega = \int_A \int_h \mathrm{d}x_3\,\mathrm{d}A$ where A denotes the area of the mid-surface. An exchange between the integration and the summation is only possible if the series converges uniformly. The proof of such a convergence becomes redundant under the assumption that the solution is physically reasonable and, hence, bounded. In addition, in view of the necessity of truncating the series anyway, upper values $m,n \in \mathbb{N}$ for the index variables k,ℓ are introduced. Exchanging the integration and summation and splitting the

integral as mentioned above allows to write (13) by means of the resultants (12) as

$$\int_\Omega \sum_{\ell=0}^{\infty} \Bigg[(\sigma_{i\alpha} x_3^\ell) \overset{\ell}{\bar{u}}_{i,\alpha} + \ell (\sigma_{i3} x_3^{\ell-1}) \overset{\ell}{\bar{u}}_i + (\sigma_{ij,j} x_3^\ell) \overset{\ell}{\bar{u}}_i + \frac{1}{\mathrm{i}\omega} \left((q_\alpha x_3^\ell) \overset{\ell}{\bar{p}}_{,\alpha} + \ell (q_3 x_3^{\ell-1}) \overset{\ell}{\bar{p}} + (q_{i,i} x_3^\ell) \overset{\ell}{\bar{p}} \right) \Bigg] \mathrm{d}\Omega \approx$$
$$\sum_{\ell=0}^{n} \int_A \left[\overset{\ell}{S}_{i\alpha} \overset{\ell}{\bar{u}}_{i,\alpha} + \ell \overset{\ell-1}{S}_{i3} \overset{\ell}{\bar{u}}_i + \overset{\ell}{T}_i \overset{\ell}{\bar{u}}_i + \frac{1}{\mathrm{i}\omega} \left(\overset{\ell}{Q}_\alpha \overset{\ell}{\bar{p}}_{,\alpha} + \ell \overset{\ell-1}{Q}_3 \overset{\ell}{\bar{p}} + \overset{\ell}{P} \overset{\ell}{\bar{p}} \right) \right] \mathrm{d}A \,. \tag{14}$$

The integration over the thickness is now hidden in the resultants and can be evaluated separately. Expression (11) has therewith been mapped onto a two-dimensional geometry consisting of the surface A.

3.2 The boundary integral

Next, the boundary integral of (9) is examined. It is given by

$$\int_{\Gamma_t} \left[t_i \bar{u}_i + \frac{1}{\mathrm{i}\omega} q_n \bar{p} \right] \mathrm{d}\Gamma_t =$$
$$\int_{A^+} \left[t_i^{(3)+} \bar{u}_i^+ + \frac{1}{\mathrm{i}\omega} q^{(3)+} \bar{p}^+ \right] \mathrm{d}A^+ + \int_{A^-} \left[t_i^{(3)-} \bar{u}_i^- + \frac{1}{\mathrm{i}\omega} q^{(3)-} \bar{p}^- \right] \mathrm{d}A^- + \int_B \left[t_i^{(\alpha)} \bar{u}_i + \frac{1}{\mathrm{i}\omega} q^{(\alpha)} \bar{p} \right] \mathrm{d}B \,. \tag{15}$$

where $t_i = \sigma_{ij} n_j$ are the components of the prescribed surface stresses and $q_n = q_i n_i$ is the normal component of the prescribed total flux on the boundary, n_i denoting the components of the outward normal vector. In (15) the boundary integral over Γ_t has been split into integrals over A^+, A^-, and B in order to cover the whole boundary of the domain (see figure 1). On $A^\pm$ the normal vector is of the form $[0,0,\pm 1]^\top$, hence,

$$(\sigma_{ij} n_j)^\pm = (\sigma_{i3} n_3)^\pm = t_i^{(3)\pm} \qquad \text{and} \qquad (q_i n_i)^\pm = (q_3 n_3)^\pm = q^{(3)\pm} \,.$$

Along B, the normal vector has the form $[n_1, n_2, 0]^\top$, hence

$$(\sigma_{ij} n_j)^B = (\sigma_{i\alpha} n_\alpha) = t_i^{(\alpha)} \qquad \text{and} \qquad (q_i n_i)^B = (q_\alpha n_\alpha) = q^{(\alpha)} \,.$$

For all quantities on A^+ and A^- the x_3-coordinate is no longer unknown and takes the values $x_3 = \frac{h}{2}$ and $x_3 = -\frac{h}{2}$, respectively. The geometry of the plate is restricted such that in an undeformed state, the two surfaces A^+ and A^- are equal to each other and to the mid-surface A. Under those assumptions the two integrals over A^+ and A^- on the right hand side of (15) can be merged to a single integral over A. With fixed x_3 the power series (10b) become

$$\begin{aligned} \bar{u}_i^+ &\approx \sum_{\ell=0}^{n} \overset{\ell}{\bar{u}}_i \left(\frac{h}{2} \right)^\ell \qquad & \bar{u}_i^- &\approx \sum_{\ell=0}^{n} \overset{\ell}{\bar{u}}_i \left(-\frac{h}{2} \right)^\ell \\ \bar{p}^+ &\approx \sum_{\ell=0}^{n} \overset{\ell}{\bar{p}} \left(\frac{h}{2} \right)^\ell \qquad & \bar{p}^- &\approx \sum_{\ell=0}^{n} \overset{\ell}{\bar{p}} \left(-\frac{h}{2} \right)^\ell . \end{aligned} \tag{16}$$

Above, the upper value n for the index variable ℓ has been introduced, hence, the series expansions become approximations of the original functions. The two integrals over $A^{\pm}$ can thus be written as

$$\int_{A^+}\left[t_i^{(3)+}\bar{u}_i^+ + \frac{1}{\mathrm{i}\omega}q^{(3)+}\bar{p}^+\right]\mathrm{d}A^+ + \int_{A^-}\left[t_i^{(3)-}\bar{u}_i^- + \frac{1}{\mathrm{i}\omega}q^{(3)-}\bar{p}^-\right]\mathrm{d}A^- \approx \sum_{\ell=0}^{n}\int_A\left[\overset{\ell}{t}{}_i^{(3)}\overset{\ell}{\bar{u}}_i + \frac{1}{\mathrm{i}\omega}\overset{\ell}{q}{}^{(3)}\overset{\ell}{\bar{p}}\right]\mathrm{d}A \tag{17}$$

where the resultants

$$\overset{\ell}{t}{}_i^{(3)} = t_i^{(3)+}\left(\frac{h}{2}\right)^{\ell} + t_i^{(3)-}\left(-\frac{h}{2}\right)^{\ell} \qquad \text{and} \qquad \overset{\ell}{q}{}^{(3)} = q^{(3)+}\left(\frac{h}{2}\right)^{\ell} + q^{(3)-}\left(-\frac{h}{2}\right)^{\ell} \tag{18}$$

have been introduced. So far, expression (17) takes into account all loadings prescribable on A, regardless of a distinction between the in-plane and the out-of-plane problem.

Contrary to the integral over A, the boundary integral over B on the right hand side of (15) contains an integration over the thickness. The variations $\bar{u}_i$ and $\bar{p}$ are replaced by the power series expansions (10b) and the resultants (12a) are introduced, yielding

$$\int_B\left[t_i^{(\alpha)}\bar{u}_i + \frac{1}{\mathrm{i}\omega}q^{(\alpha)}\bar{p}\right]\mathrm{d}B \approx \sum_{\ell=0}^{n}\int_C\left[(\overset{\ell}{S}_{i\alpha}n_\alpha)\overset{\ell}{\bar{u}}_i + \frac{1}{\mathrm{i}\omega}(\overset{\ell}{Q}_\alpha n_\alpha)\overset{\ell}{\bar{p}}\right]\mathrm{d}C\,. \tag{19}$$

With the surface integrals (14) and (17) (note that the former one arises from the 3d domain integral, whereas the latter arises from both boundary integrals over $A^{\pm}$) and the boundary integral (19), the three-dimensional work equation (9) has been mapped onto the two-dimensional geometry. The full expression reads

$$\begin{aligned}\sum_{\ell=0}^{n}\int_A\left[\overset{\ell}{S}_{i\alpha}\overset{\ell}{\bar{u}}_{i,\alpha} + \ell\overset{\ell-1}{S}_{i3}\overset{\ell}{\bar{u}}_i + \overset{\ell}{T}_i\overset{\ell}{\bar{u}}_i + \frac{1}{\mathrm{i}\omega}\left(\overset{\ell}{Q}_\alpha\overset{\ell}{\bar{p}}_{,\alpha} + \ell\overset{\ell-1}{Q}_3\overset{\ell}{\bar{p}} + \overset{\ell}{P}\overset{\ell}{\bar{p}}\right)\right]\mathrm{d}A = \\ \sum_{\ell=0}^{n}\int_A\left[\overset{\ell}{t}{}_i^{(3)}\overset{\ell}{\bar{u}}_i + \frac{1}{\mathrm{i}\omega}\overset{\ell}{q}{}^{(3)}\overset{\ell}{\bar{p}}\right]\mathrm{d}A + \sum_{\ell=0}^{n}\int_C\left[(\overset{\ell}{S}_{i\alpha}n_\alpha)\overset{\ell}{\bar{u}}_i + \frac{1}{\mathrm{i}\omega}(\overset{\ell}{Q}_\alpha n_\alpha)\overset{\ell}{\bar{p}}\right]\mathrm{d}C\,.\end{aligned} \tag{20}$$

It should be kept in mind that equation (20) still holds for a three-dimensional continuum. Only some geometrical restrictions and a not closer specified truncation of the series expansions have been imposed so far.

4 The resultants

After the two-dimensional work equation has been formulated, the plate problem can be retrieved. As it turns out, equation (20) can actually be decoupled into an in-plane (i.e., disc) and an out-of-plane (i.e., plate) problem. In order to accomplish this decoupling the quantities related to the respective problems have to be identified. For distinguishing the plate and disc quantities the sets of even and odd numbers are introduced and defined as

$$\mathbb{E} = \{a\,|\,a = 2a',\, a' \in \mathbb{N}\} \qquad \mathbb{O} = \{a\,|\,a = 2a' + 1,\, a' \in \mathbb{N}\}\,.$$

It lies in the nature of the plate that its mid-surface doesn't experience any in-plane motion, hence, every point on the mid-surface is only allowed to move in x_3-direction. This discards the $\overset{0}{u}_\alpha$ component of the series expansion (10) and with it any term of even order $\overset{k}{u}_\alpha$, $k \in \mathbb{E}$, since an integration over the thickness of those terms would always result into a nonzero in-plane displacement of the mid-surface. Integrating the terms of odd order $\overset{k}{u}_\alpha x_3^k$, $k \in \mathbb{O}$, however, leads to a zero total in-plane displacement despite $\overset{k}{u}_\alpha x_3^k \neq 0$ for $x_3 \neq 0$. In that case, the quantities $\overset{k}{u}_\alpha$ describe rotations of the cross section. The linear term keeps the cross section undeformed, whereas terms of higher order ($k = 3, 5 \ldots$) include warping effects.

On the other hand, the terms $\overset{k}{u}_3$, $k \in \mathbb{E}$ have to be considered since they describe a pure out-of-plane displacement, where the constant term $\overset{0}{u}_3$ is the vertical displacement of the mid-surface and the higher terms of even order $\overset{k}{u}_3$ describe the magnitude of the respective thickening and thinning of the two plate halves during bending.

The constant pressure term $\overset{0}{p}$ demands constant in-plane stresses over the thickness in order to keep balance. Such stresses, however, are not allowed in a pure plate formulation. All pressure terms of higher even order share this property. Hence, for plate calculations, only the odd pressure terms $\overset{k}{p}$, $k \in \mathbb{O}$ are allowed. They describe the pressure distribution over the thickness of linear, cubic, quintic order and so on.

The same distinction also applies to the functions of variation. The plate and disc quantities resulting from the series expansions (10) are summarized in table 1.

	$\overset{k}{u}_\alpha$, $\overset{\ell}{\bar{u}}_\alpha$	$\overset{k}{u}_3$, $\overset{\ell}{\bar{u}}_3$	$\overset{k}{p}$, $\overset{\ell}{\bar{p}}$
plate	$k, \ell \in \mathbb{O}$	$k, \ell \in \mathbb{E}$	$k, \ell \in \mathbb{O}$
disc	$k, \ell \in \mathbb{E}$	$k, \ell \in \mathbb{O}$	$k, \ell \in \mathbb{E}$

Table 1: Separation of plate and disc quantities

All resultants (12) are functions of u_i and p and can either be related to the plate or to the disc problem. Since the procedure is basically identical, only the resultants related to the plate problem will be evaluated here. Therefore, the expressions from section 2 are used to write the resultants as functions of u_i and p, which then are replaced by the series expansions (10). As already mentioned earlier, the sum and the integral can be exchanged under the condition that the sum converges uniformly or it is finite. Again, the latter case is sufficient. The integration over the thickness represents no difficulty anymore. In order to consider only the plate problem, only the respective quantities according to table 1 are used.

With the evaluated resultants (34)−(41) (see appendix A) the left hand side of (20), finally, reduces to the aimed two-dimensional form. The dependency on x_3 has been completely eliminated.

As noted above, the evaluated resultants only cover the plate problem. Hence, the right hand side of (20) must be evaluated accordingly. At this point it is essential to realize which quantities can be prescribed in order to model a pure plate problem and which quantities would introduce effects related to the disc problem. In a first instance, the surface integral (17) is investigated.

More explicitly, it is written

$$\sum_{\ell=0}^{n}\int_A \left[\overset{\ell}{t}{}_i^{(3)}\,\overset{\ell}{\bar{u}}_i + \frac{1}{\mathrm{i}\omega}\overset{\ell}{q}{}^{(3)}\,\overset{\ell}{\bar{p}}\right]\mathrm{d}A = \sum_{\ell=0}^{n}\int_A \left[\overset{\ell}{t}_\alpha\,\overset{\ell}{\bar{u}}_\alpha + \overset{\ell}{t}_3\,\overset{\ell}{\bar{u}}_3 + \frac{1}{\mathrm{i}\omega}\overset{\ell}{q}\,\overset{\ell}{\bar{p}}\right]\mathrm{d}A\,. \tag{21}$$

On the right hand side of (21) and in the following, the superscript $^{(3)}$ denoting the direction of the normal vector is neglected since no danger of confusion is given. According to the definition (18), the resultants in (21) can be written as

$$\begin{aligned}
&\overset{\ell}{\chi} = \left(\frac{h}{2}\right)^{\ell}\overset{0}{\chi} \qquad \text{for} \quad \ell\in\mathbb{E} \qquad \text{with} \quad \overset{0}{\chi} = \chi^+ + \chi^- \\
&\overset{\ell}{\chi} = \left(\frac{h}{2}\right)^{\ell}\overset{1}{\chi} \qquad \text{for} \quad \ell\in\mathbb{O} \qquad \text{with} \quad \overset{1}{\chi} = \frac{h}{2}\left(\chi^+ - \chi^-\right)
\end{aligned} \tag{22}$$

where χ stands for either t_α, t_3, or q and $\chi^\pm$ stands for the respective prescribed quantity on $A^\pm$. Considering the orders of the variations which the resultants are multiplied with, reveals that the plate related quantities are

$$\begin{aligned}
&\overset{\ell}{t}_3 = \left(\frac{h}{2}\right)^{\ell}\overset{0}{t}_3 \quad \text{for} \quad \ell\in\mathbb{E} \\
&\overset{\ell}{t}_\alpha = \left(\frac{h}{2}\right)^{\ell}\overset{1}{t}_\alpha \quad \text{and} \quad \overset{\ell}{q} = \left(\frac{h}{2}\right)^{\ell}\overset{1}{q} \quad \text{for} \quad \ell\in\mathbb{O}
\end{aligned} \tag{23}$$

whereas the disc quantities are

$$\begin{aligned}
&\overset{\ell}{t}_3 = \left(\frac{h}{2}\right)^{\ell}\overset{1}{t}_3 \quad \text{for} \quad \ell\in\mathbb{O} \\
&\overset{\ell}{t}_\alpha = \left(\frac{h}{2}\right)^{\ell}\overset{0}{t}_\alpha \quad \text{and} \quad \overset{\ell}{q} = \left(\frac{h}{2}\right)^{\ell}\overset{0}{q} \quad \text{for} \quad \ell\in\mathbb{E}\,.
\end{aligned} \tag{24}$$

Apparently, prescribing only stresses in x_3-direction does not guarantee a pure plate problem. On the other hand, in-plane stresses may be prescribed on the surfaces. The surface flux can activate the disc problem, too. In order to formulate a pure plate problem it has to be assured that the prescribed surface stresses and fluxes fulfill

$$t_3^+ = t_3^- \qquad t_\alpha^+ = -t_\alpha^- \qquad q^+ = -q^-\,. \tag{25}$$

With (22) it can be easily verified that those conditions force the disc resultants (24) to be equal to zero. If one of the conditions (25) are not fulfilled, the plate calculation is still valid, but in order to reconstruct the real state of stress in the structure, the disc problem has to be additionally considered.

The boundary integral over C in (20) takes care of the prescribed quantities along the boundary B. This boundary curve lives in the (x_1,x_2)-plane, hence, the component n_3 of its normal vector $\mathbf{n}$ is zero everywhere. This yields

$$\sum_{\ell=0}^{n}\int_C \left[(\overset{\ell}{S}_{i\alpha}n_\alpha)\,\overset{\ell}{\bar{u}}_i + \frac{1}{\mathrm{i}\omega}(\overset{\ell}{Q}_\alpha n_\alpha)\,\overset{\ell}{\bar{p}}\right]\mathrm{d}C = \sum_{\ell=0}^{n}\int_B \left[(\overset{\ell}{S}_{\alpha\beta}n_\beta)\,\overset{\ell}{\bar{u}}_\alpha + (\overset{\ell}{S}_{3\beta}n_\beta)\,\overset{\ell}{\bar{u}}_3 + \frac{1}{\mathrm{i}\omega}(\overset{\ell}{Q}_\alpha n_\alpha)\,\overset{\ell}{\bar{p}}\right]\mathrm{d}B\,. \tag{26}$$

Expression (26) still covers all boundary conditions related to both the plate and the disc. Again, the order of the variation tells which quantity is related to which problem. The plate quantities turn out to be

$$\begin{aligned}
&\overset{\ell}{S}_{\alpha\beta}n_\beta = \overset{\ell}{S}_{\alpha 1}n_1 + \overset{\ell}{S}_{\alpha 2}n_2 = \overset{\ell}{M}_\alpha && \text{for} \quad \ell \in \mathbb{O} \\
&\overset{\ell}{S}_{3\beta}n_\beta = \overset{\ell}{S}_{31}n_1 + \overset{\ell}{S}_{32}n_2 = \overset{\ell}{V} && \text{for} \quad \ell \in \mathbb{E} \\
&\overset{\ell}{Q}_\alpha n_\alpha = \overset{\ell}{Q}_1 n_1 + \overset{\ell}{Q}_2 n_2 = \overset{\ell}{Q} && \text{for} \quad \ell \in \mathbb{O}
\end{aligned} \tag{27}$$

with $\overset{1}{M}_\alpha$ being the moments around the x_α-axes, $\overset{0}{V}$ being the shear force and $\overset{1}{Q}$ being some kind of "flux moment". This "flux moment", together with all higher order quantities have no counterpart in classical theories. Instead of prescribing M_1 and M_2 on an arbitrary boundary curve it is more natural to prescribe the bending moment M_n (i.e., the moment around the tangential vector) and the twisting moment M_s (i.e., the moment around the normal vector) and to transform them back by

$$\begin{bmatrix} M_1 \\ M_2 \end{bmatrix} = \begin{bmatrix} n_1 & -n_2 \\ n_2 & n_1 \end{bmatrix} \begin{bmatrix} M_n \\ M_s \end{bmatrix}.$$

For the plate problem, the general form of the two-dimensional work equation (20) is thus reduced to

$$\begin{aligned}
&\sum_{\substack{\ell=0 \\ \ell\in\mathbb{E}}}^{n} \int_A \left[\overset{\ell}{S}_{3\alpha} \overset{\ell}{\bar{u}}_{3,\alpha} + \ell \overset{\ell-1}{S}_{33} \overset{\ell}{\bar{u}}_3 + \overset{\ell}{T}_3 \overset{\ell}{\bar{u}}_3 \right] \mathrm{d}A + \\
&\sum_{\substack{\ell=1 \\ \ell\in\mathbb{O}}}^{n} \int_A \left[\overset{\ell}{S}_{\alpha\beta} \overset{\ell}{\bar{u}}_{\alpha,\beta} + \ell \overset{\ell-1}{S}_{\alpha 3} \overset{\ell}{\bar{u}}_\alpha + \overset{\ell}{T}_\alpha \overset{\ell}{\bar{u}}_\alpha + \frac{1}{\mathrm{i}\omega} \left(\overset{\ell}{Q}_\alpha \overset{\ell}{\bar{p}}_{,\alpha} + \ell \overset{\ell-1}{Q}_3 \overset{\ell}{\bar{p}} + \overset{\ell}{P} \overset{\ell}{\bar{p}} \right) \right] \mathrm{d}A = \\
&\sum_{\substack{\ell=0 \\ \ell\in\mathbb{E}}}^{n} \int_A \overset{\ell}{t}_3 \overset{\ell}{\bar{u}}_3 \, \mathrm{d}A + \sum_{\substack{\ell=1 \\ \ell\in\mathbb{O}}}^{n} \int_A \left[\overset{\ell}{t}_\alpha \overset{\ell}{\bar{u}}_\alpha + \frac{1}{\mathrm{i}\omega} \overset{\ell}{q}_3 \overset{\ell}{\bar{p}} \right] \mathrm{d}A + \sum_{\substack{\ell=0 \\ \ell\in\mathbb{E}}}^{n} \int_C \overset{\ell}{V}_3 \overset{\ell}{\bar{u}}_3 \, \mathrm{d}C + \sum_{\substack{\ell=1 \\ \ell\in\mathbb{O}}}^{n} \int_C \left[\overset{\ell}{M}_\alpha \overset{\ell}{\bar{u}}_\alpha + \frac{1}{\mathrm{i}\omega} \overset{\ell}{Q}_3 \overset{\ell}{\bar{p}} \right] \mathrm{d}C .
\end{aligned} \tag{28}$$

The work equation for the disc can be obtained in the same way.

One important point not discussed so far remains the question about the truncation of the series. As mentioned in the introduction, Kienzler [12, 13] shows how to obtain the classical elastostatic plate equations by using series expansions in thickness direction. Therefore, he evaluates all resultants similarly as shown in appendix A and considers only those terms which are multiplied by up to a specific order of the plate parameter $c^2 = h^2/12$. By neglecting all terms multiplied by c^4 and higher the *first order approximation* is obtained which can be reduced to the classical Kirchhoff plate equation. Neglecting all terms multiplied by c^6 and higher leads to a larger system, i.e., the *second order approximation*, which again can be reduced to one single equation describing shear-deformable plates. Hence, it would seem natural to use the same technique for the poroelastodynamic system presented here. The critical point, however, lies in reducing the system of partial differential equations to one single equation since the factor c^2 influences crucially the meaning of the expressions in the system. As an example, the equation

$$w_{,\alpha} + \psi_\alpha = 0$$

shall be mentioned, where $\overset{0}{u}_3 := w$ and $\overset{1}{u}_\alpha := \psi_\alpha$. This equation states that the gradient of the vertical displacement w is equal to the rotations ψ_α of the cross section, hence, it expresses the Kirchhoff normal hypothesis. Independent of the level of approximation, this equation can be found in every system. In the case of the *first* and *second order approximations* it takes the form

$$c^2(w_{,\alpha} + \psi_\alpha) + \mathcal{O}(c^4) = 0 \qquad \text{and} \qquad c^4(w_{,\alpha} + \psi_\alpha) + \mathcal{O}(c^6) = 0\,,$$

respectively. Clearly, the second equation above cannot be interpreted as the Kirchhoff normal hypothesis since it belongs to a system describing shear-deformable plates. Additionally, neither of the two equations can be explicitly resolved for one or the other function, since this would demand dividing by c^2 (or c^4) which would cause the terms of higher order to be not negligible anymore.

Within the framework presented by Kienzler, this somehow strange behavior makes perfect sense and the systems can be reduced by following a certain approach. This may, however, become a cumbersome procedure for systems of higher order, even in elastostatics. Solving the full system right away without reducing it also requires special routines in order to handle those difficulties. Moreover, in contrast to the elastostatic case, the insights deducible from the *zeroth order approximation* become less obvious in the poroelastic case.

Adopting appropriate measures should almost undoubtedly allow a numerical solution of the system proposed by Kienzler. Within this work, however, such measures have not been investigated thoroughly. Instead, another way of truncating the series has been applied which avoids the main difficulties encountered above. Therefore, the series are truncated with respect to some arbitrary value $m = n$ for the unknown quantities. Although the systems obtained in this way do not yield the classical plate equations, the results presented in section 6 justify this approach.

5 Finite element formulation

Equation (28) represents the weak form of the problem to be solved, with the functions of variation being the usual test-functions. Hence, the system can be treated by the finite element method.

After having discussed how to truncate the series at the end of the previous chapter, now the question arises where to truncate it, i.e., which value $m = n$ should be chosen. The more unknown functions are considered, the better the three-dimensional equations are approximated but, clearly, the computational effort increases.

The goal is to obtain good results and to keep the computational effort as low as possible. This means that a convenient order $m = n$ for the series expansions has to be chosen. The resultants then are evaluated considering all quantities up to that specific order. A first guess for the minimal needed order is obtained by considering the strong form of the problem. It can be easily obtained by integrating the weak form by parts, such that the derivatives in the variations are shifted to the resultants and extracting the partial differential equations. The so obtained system of PDEs may be reduced to one single equation or to a set of equations containing only the functions of interest (e.g., the vertical deflection and the pore pressure). The advantage is that the so obtained equations can easily be compared to classical plate equations and, hence, their validity can be estimated.

In the elastodynamic case the strong form of the linear ansatz, i.e., only $\overset{0}{u}_3$ and $\overset{1}{u}_\alpha$ are considered, corresponds to the classical C^0 approach for plates (see e.g., [10]), however, with slightly different parameters. Hence, the equation which is obtained after eliminating the rotations shows a different plate stiffness compared to the one known from the Kirchhoff or Mindlin plate equations. Expanding to the quadratic ansatz, i.e., by adding $\overset{2}{u}_3$ to the system, eliminates this mismatch and the "correct" stiffness is obtained. At the same time, however, additional terms are introduced so that this system represents some sort of extended version of the classical C^0 approach. Independent of the level m of approximation only first derivatives appear in the weak formulation so that C^0-continuity is always sufficient.

Eliminating some unknowns, e.g., the rotations as above, obviously reduces the number of equations in the system. However, it is still more convenient to solve the full system because the elimination increases the order of the resulting PDEs and their solution becomes very cumbersome. In the poroelastic case even the linear ansatz leads to a combination of a forth and a second order PDE for $\overset{0}{u}_3$ and $\overset{1}{p}$ or, alternatively, to a sixth order PDE for $\overset{0}{u}_3$, which requires C^1-continuity for the former, or even C^2-continuity for the latter case.

As a limiting case, the poroelastic formulation must be able to model the elastic problem correctly. Hence, taking into account the insights gained above, it can be stated that for the general case at least the quadratic terms of the series are needed to obtain results not contradicting the classical theories.

The Bubnov-Galerkin formulation of the problem is obtained by replacing the unknown functions of the weak form by finite dimensional approximations

$$\begin{aligned}
\overset{k}{u}_3 &\to \overset{k}{u}{}^h_3 = \sum_{i\in\eta} \overset{k}{u}_{3i}\,\varphi_i & \qquad \overset{k}{\bar{u}}_3 &\to \overset{k}{\bar{u}}{}^h_3 = \sum_{i\in\eta} \overset{k}{\bar{u}}_{3i}\,\varphi_i \\
\overset{k}{u}_\alpha &\to \overset{k}{u}{}^h_\alpha = \sum_{i\in\eta} \overset{k}{u}_{\alpha i}\,\phi_{\alpha i} & \qquad \overset{k}{\bar{u}}_\alpha &\to \overset{k}{\bar{u}}{}^h_\alpha = \sum_{i\in\eta} \overset{k}{\bar{u}}_{\alpha i}\,\phi_{\alpha i} \\
\overset{k}{p} &\to \overset{k}{p}{}^h = \sum_{i\in\eta} \overset{k}{p}_i\,\vartheta_i & \qquad \overset{k}{\bar{p}} &\to \overset{k}{\bar{p}}{}^h = \sum_{i\in\eta} \overset{k}{\bar{p}}_i\,\vartheta_i
\end{aligned} \tag{29}$$

where η denotes the set of degrees of freedom for the respective function. Since only C^0-continuity is required, Lagrangian shape functions on quadrilateral elements are used. For the 3d poroelastic system it is usual to approximate the displacement field u_i by biquadratic shape functions, whereas the pore pressure field p is approximated bilinearly [16]. The same approximations are applied here which means that all displacement quantities are approximated by biquadratic shape functions and all pressure quantities by bilinear shape functions. Numerical tests show that using only bilinear shape functions results into an extremely slow convergence rate even for low frequencies. Using biquadratic shape functions for $\overset{k}{u}_3$ and keeping bilinear functions for the other unknowns approximates the low-frequency-solution well even for coarse meshes. In this case, however, a very fine mesh to determine higher eigenfrequencies is necessary. The use of biquadratic shape functions for $\overset{k}{u}_3$ as well as for $\overset{k}{u}_\alpha$ alleviates this problem.

In the present work the quadratic ansatz is treated enriched by the cubic term for the pore pressure. This means that the unknown functions considered are $\overset{0}{u}_3, \overset{2}{u}_3, \overset{1}{u}_\alpha, \overset{1}{p}$, and $\overset{3}{p}$. By truncating the weak form (28) accordingly and inserting the approximations (29), a linear system of

equations is obtained. In the following, the unknown coefficients in (29) are written as

$$\boldsymbol{u}_3 := \begin{bmatrix} \overset{0}{\boldsymbol{u}}_3 \\ \overset{2}{\boldsymbol{u}}_3 \end{bmatrix} := \begin{bmatrix} \begin{bmatrix} \overset{0}{u}_{3i} \end{bmatrix}_{i\in\eta} \\ \begin{bmatrix} \overset{2}{u}_{3i} \end{bmatrix}_{i\in\eta} \end{bmatrix} \qquad \boldsymbol{u}_\alpha := \overset{1}{\boldsymbol{u}}_\alpha := \begin{bmatrix} \overset{1}{u}_{\alpha i} \end{bmatrix}_{i\in\eta} \qquad \boldsymbol{p} := \begin{bmatrix} \overset{1}{\boldsymbol{p}} \\ \overset{3}{\boldsymbol{p}} \end{bmatrix} := \begin{bmatrix} \begin{bmatrix} \overset{1}{p}_i \end{bmatrix}_{i\in\eta} \\ \begin{bmatrix} \overset{3}{p}_i \end{bmatrix}_{i\in\eta} \end{bmatrix} . \tag{30}$$

The system of equations can then be written in the compact form

$$\begin{bmatrix} \mathbf{A} & \mathbf{B}_\alpha & \mathbf{C} \\ \mathbf{B}_\alpha^\top & \mathbf{D}_{\alpha\beta} & \mathbf{E}_\alpha \\ \mathbf{C}^\top & \mathbf{E}_\alpha^\top & \mathbf{F} \end{bmatrix} \begin{bmatrix} \boldsymbol{u}_3 \\ \boldsymbol{u}_\alpha \\ \boldsymbol{p} \end{bmatrix} = \begin{bmatrix} \boldsymbol{f} \\ \boldsymbol{g}_\alpha \\ \boldsymbol{h} \end{bmatrix} . \tag{31}$$

The submatrices on the left hand side are the discrete versions of the continuous differential operators encountered in the weak formulation. The right hand side contains all prescribed quantities on the surface A and along the boundary curve C. Its solution delivers the nodal values $\boldsymbol{u}_3, \boldsymbol{u}_\alpha$, and $\boldsymbol{p}$ in the discretized domain.

All higher order terms can easily be incorporated into the system (31) by simply adding the additional unknowns into the respective vector of (30).

6 Numerical results

6.1 System specification

In order to validate the presented plate formulation a clamped quadratic plate of $4.0 \times 4.0 \times 0.2\,[\mathrm{m}]$ is considered. Clamped means that all displacement quantities of any order are assumed to be zero on the boundary C. The origin of the underlying coordinate system is placed such that the plate domain occupies the region $x_1 \in [-2,2]$, $x_2 \in [-2,2]$ and $x_3 \in [-0.1,0.1]$. The plate is excited by a uniformly distributed load on A with $t_3^+ = t_3^- = 0.5\,\mathrm{kN/m^2}$. The load is constant in frequency-domain which corresponds to a harmonic excitation in time. Figure 2 shows the respective discretizations.

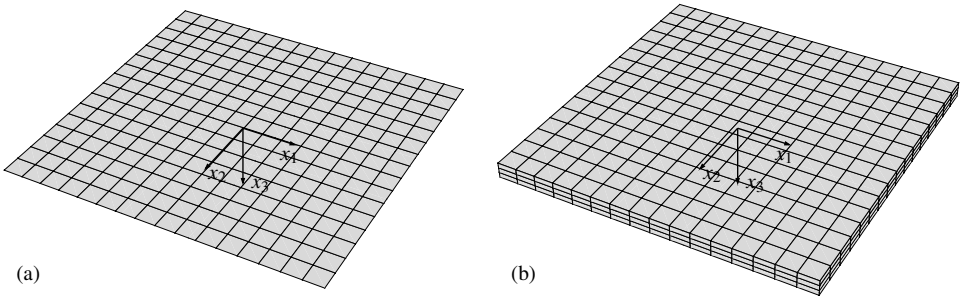

Figure 2: Spatial discretization of the considered plate. (a) 2d - Quad9, 16×16 and (b) 3d - Hex20, $16 \times 16 \times 3$

The plate is, firstly, compared to the three-dimensional solution and, secondly, to two elastic calculations representing lower and upper bounds for the poroelastic solution. Finally, the distribution of the four degrees of freedom over the thickness are discussed and compared to the 3d solution.

	poroelastic	elastic drained	elastic undrained
Young's modulus $E[\mathrm{kN/m^2}]$	1.44×10^7	1.44×10^7	1.60×10^7
Poisson's ratio ν[-]	0.2	0.2	0.335
density $\rho[\mathrm{kg/m^3}]$	2.458	2.458	2.458
porosity ϕ[-]	0.19	-	-
fluid density $\rho_f[\mathrm{kg/m^3}]$	1.000	-	-
solid bulk modulus $K_s[\mathrm{kN/m^2}]$	3.60×10^7	-	-
fluid bulk modulus $K_f[\mathrm{kN/m^2}]$	3.30×10^6	-	-
permeability $\kappa[\mathrm{m^4/kNs}]$	1.90×10^{-7}	-	-

Table 2: Material data for Berea sandstone and corresponding drained and undrained elastic cases

6.2 Plate *versus* 3d

The first validation is done by comparing the numerical solution of the plate to the numerical solution of the three-dimensional poroelastic system (8). For the 3d calculation Hex20 elements are used. The displacement field is approximated by quadratic Lagrangian shape functions whereas the pore pressure is approximated by linear Lagrangian shape functions. For the plate, Quad9 elements are used. All displacement quantities are approximated by biquadratic Lagrangian shape functions, whereas for all pore pressure quantities bilinear Lagrangian shape functions are used.

For the 3d calculation it is essential to apply the load in the "right" way. The load has been specified as $t_3^+ = t_3^- = 0.5\,\mathrm{kN/m^2}$ although for the plate calculation the distinction between t_3^+ and t_3^- is not relevant since both quantities act on the same surface A. In contrast to that, such a distinction becomes important in the 3d case since now the two surfaces A^+ and A^- are separated in space. As pointed out in section 4, a vertical load which is not applied symmetrically to the mid-surface would activate the disc problem and, hence, introduce unwanted stresses in the structure.

The comparison of the two solutions is depicted in figure 3. The vertical deflection of the middle-point of the plate at $x_1 = x_2 = 0$ and the middle-point of the 3d structure at $x_1 = x_2 = x_3 = 0$ are plotted versus the angular frequency.

The 3d solution shows the same behavior as the plate. It can be observed that the vertical deflection is prevented from reaching infinity when approaching the eigenfrequency. This illustrates the damping behavior of the poroelastic system (the inverse peaks are just due to the use of absolute values and the different amplitudes at those peaks are just accidental due to the finite discretization over the frequency.) Up to a frequency of approximately $1000[\mathrm{rad/s}]$ the two solutions match perfectly. For larger frequencies the plate reveals to be slightly stiffer. This may

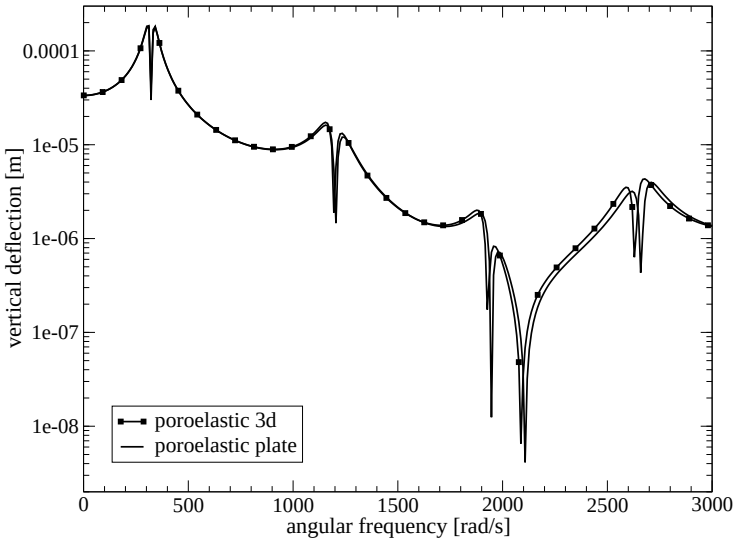

Figure 3: Comparison of the plate and the 3d solution

be explained by the fact that the original degrees of freedom u_i and p are only approximated and, hence, additional constraints are introduced compared to the 3d formulation.

6.3 Poroelastic plate *versus* elastic drained/undrained plate

Next, the so-called elastic drained and undrained cases are introduced. As already mentioned they represent theoretical upper and lower bounds for the poroelastic solution. The drained case assumes that the interstitial fluid has enough time to equilibrate its pore pressure with the pressure imposed at the boundary. This behavior is expected for a slowly applied load, hence, for the quasi-static case and lower frequencies. On the other hand, the undrained case assumes that the interstitial fluid has no time to move at all which represents the systems response after an instantaneously applied load and, hence, represents the behavior expected for higher frequencies. It is obvious that the undrained plate is stiffer than the drained one. The poroelastic solution should lie somewhere in between. For the calculation, Berea Sandstone is chosen. The material data are given in table 2 (see [9] for details regarding the drained and undrained cases and their material properties).

Figure 4 shows the vertical deflection $\overset{0}{u}_3$ of the plates middle-point located at $x_1 = x_2 = 0$ in dependence of the angular frequency. Note that the four depicted eigenfrequencies are not the first four eigenfrequencies of the system but only the first four appearing.

Again, contrary to both elastic cases, in the poroelastic solution the vertical deflection is prevented from reaching infinity when approaching the eigenfrequency. In a quasi-static neighborhood up to a frequency of, say, $200[\mathrm{rad}/\mathrm{s}]$, the difference between the poroelastic and the elastic-drained solution is negligible (see the zoom in figure 4). The larger the frequency, the more the poroelastic solution is shifted towards the elastic-undrained one. This is in accordance to the expected behavior described above.

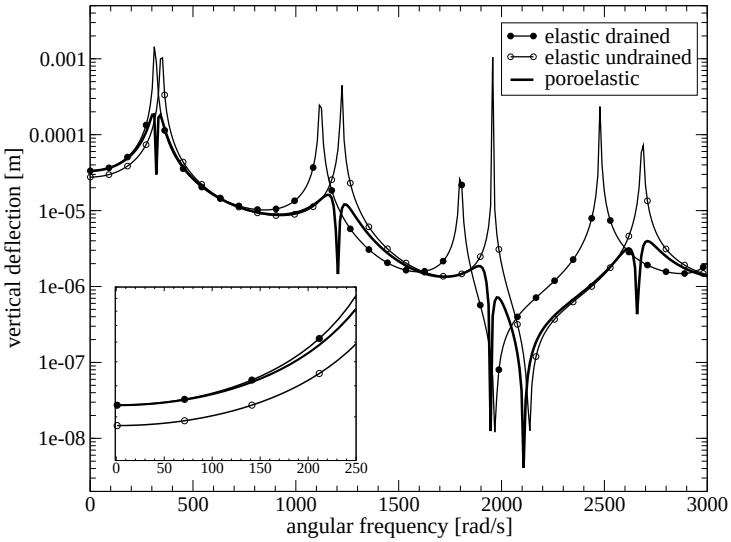

Figure 4: Comparison of the poroelastic and both drained and undrained solutions

6.4 Distribution over the thickness

Figure 3 only compares the vertical deflections $\overset{0}{u}_3(0,0)$ of the plate and $u_3(0,0,0)$ of the 3d structure. Since the plate formulation has been developed to approximate a 3d model, all other plate quantities are expected to coincide well. The four degrees of freedom consist of the three displacement fields $u_i(x_1,x_2,x_3)$ and the pore pressure $p(x_1,x_2,x_3)$. The 3d model is directly solved for all of these four dofs. The proposed plate formulation, however, does not provide a solution for any of these dofs right away since the dependency on the thickness coordinate x_3 is not considered. The dofs u_i and p have to be reconstructed by substituting the solutions of the single plate quantities back into the series expansions.

In order to get a better comparison, the discretization in x_3-direction of the 3d structure has been increased from 3 to 5 elements over the thickness for this calculation.

The present formulation has taken into account the quantities $\overset{0}{u}_3, \overset{2}{u}_3, \overset{1}{u}_1, \overset{1}{u}_2, \overset{1}{p}, \overset{3}{p}$. The calculated values are summarized in the tables 3 and 4 at $(x_1,x_2) = (-0.5,-1.0)$.

x_3	u_1[m]	u_2[m]	u_3[m]	p[kN/m^2]
0.10	$8.07998 \cdot 10^{-7}$	$2.10318 \cdot 10^{-6}$	$-1.82117 \cdot 10^{-5}$	$7.23695 \cdot 10^{-5}$
0.06	$4.82737 \cdot 10^{-7}$	$1.25270 \cdot 10^{-6}$	$-1.82317 \cdot 10^{-5}$	$5.86240 \cdot 10^{-5}$
0.02	$1.60618 \cdot 10^{-7}$	$4.16251 \cdot 10^{-7}$	$-1.82417 \cdot 10^{-5}$	$2.23166 \cdot 10^{-5}$
-0.02	$-1.60618 \cdot 10^{-7}$	$-4.16251 \cdot 10^{-7}$	$-1.82417 \cdot 10^{-5}$	$-2.23166 \cdot 10^{-5}$
-0.06	$-4.82737 \cdot 10^{-7}$	$-1.25270 \cdot 10^{-6}$	$-1.82317 \cdot 10^{-5}$	$-5.86240 \cdot 10^{-5}$
-0.10	$-8.07998 \cdot 10^{-7}$	$-2.10318 \cdot 10^{-6}$	$-1.82117 \cdot 10^{-5}$	$-7.23695 \cdot 10^{-5}$

Table 3: 3d calculation: Values at the nodes along the thickness fiber at $(x_1,x_2) = (-0.5,-1.0)$

When substituted back into the series expansions the following expressions for u_i and p are

$\overset{\ell}{u}_3$	$\overset{\ell}{u}_\alpha$	$\overset{\ell}{p}$
$\overset{0}{u}_3 = -1.811 \cdot 10^{-5}$	$\overset{1}{u}_1 = 8.043 \cdot 10^{-6}$	$\overset{1}{p} = 1.179 \cdot 10^{-3}$
$\overset{2}{u}_3 = 3.138 \cdot 10^{-6}$	$\overset{1}{u}_2 = 2.094 \cdot 10^{-5}$	$\overset{3}{p} = -3.969 \cdot 10^{-2}$

Table 4: Plate calculation: Values for the unknown quantities at $(x_1, x_2) = (-0.5, -1.0)$

obtained

$$\begin{aligned} u_1(x_i) &= \overset{1}{u}_1(x_\alpha) x_3 \\ u_2(x_i) &= \overset{1}{u}_2(x_\alpha) x_3 \\ u_3(x_i) &= \overset{0}{u}_3(x_\alpha) + \overset{2}{u}_3(x_\alpha) x_3^2 \\ p(x_i) &= \overset{1}{p}(x_\alpha) x_3 + \overset{3}{p}(x_\alpha) x_3^3 . \end{aligned} \tag{32}$$

The quantities in (32) can now be compared to those obtained from the 3d solution. Figure 5 shows the distribution over the thickness of the four dofs at $(x_1, x_2) = (-0.5, -1.0)$ for a low frequency. Obviously, the functions in (32) are continuous in x_3 whereas the 3d model delivers the solution on discrete points over the thickness.

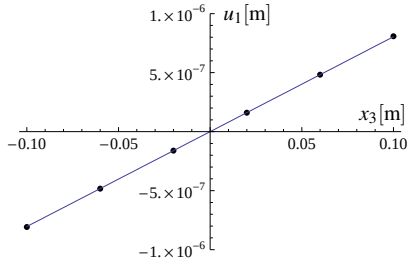

(a) displacement u_1 in x_1-direction

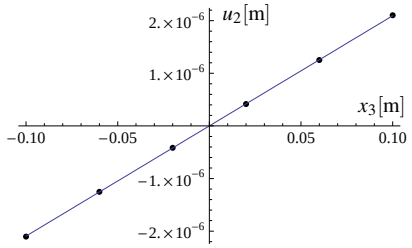

(b) displacement u_2 in x_2-direction

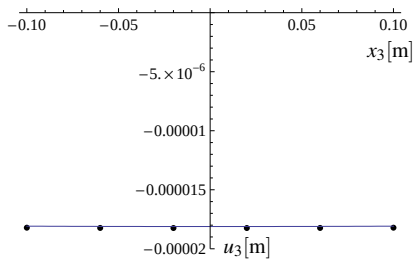

(c) vertical deflection w in x_3-direction

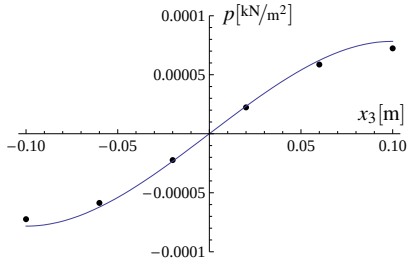

(d) pore pressure p

Figure 5: Plate solution versus 3d solution - distribution over the thickness

The two figures 5a and 5b show the two in-plane displacements u_1 and u_2. According to equation (32), the plate solution gives a linear function in x_3. The discrete 3d solution shows the exact same linear distribution. This result also confirms the assumption not to consider the cubic terms in the series expansions for both in-plane displacements. The linear term is absolutely sufficient.

The out-of-plane displacement u_3 is depicted in figure 5c and shows an excellent agreement with the 3d solution. Its quadratic distribution is made visible in figure 6. The apparent discrepancy is only due to the small data range used for this plot compared to 5c. In fact, both solutions only differ by a constant value amounting to 0.7% and the quadratic distribution over the thickness is matched perfectly.

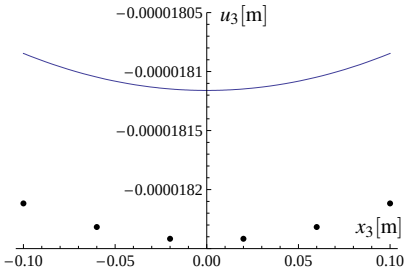

Figure 6: Vertical deflection u_3 - zoom on data range

Figure 5d shows the pore pressure p. Again, very good results for its distribution are obtained. In contrast to both the in-plane displacements, this figure clearly shows the importance of incorporating the cubic term for the pore pressure.

Calculations performed on larger frequencies show a similar agreement with the 3d model. In order to get matchable results, however, the slight frequency shift noticeable in figure 3 has to be taken into consideration. Also, the in-plane displacements reveal their cubic distribution over the thickness, although still negligible within the considered frequency range.

The plate and the 3d formulation have been implemented using the open source finite element library *libmesh* [14]. On the same machine, the plate calculation could be performed around ten times faster than the 3d calculation.

7 Conclusions

In this work, Biot's three-dimensional system of equations in frequency domain is mapped onto a two-dimensional geometry by approximating the degrees of freedom, in this case the displacement field u_i and the pore pressure field p, by power series expansions in thickness direction which then allows an integration over the thickness and, hence, reduces the spatial dimension of the problem. The in-plane and the out-of-plane problems decouple naturally. After working through the algebra, different level of approximations can be extracted. At least a quadratic order in the series expansions is needed to obtain the classical plate stiffness. However, as shown in the results, not one specific approximation order m has to be chosen, but rather all dofs may be approximated differently. This allows truncating the u_3-series after the quadratic term, both u_α-series after the linear term and the p-series after the cubic term.

The comparison with the full 3d model shows very good agreement in every sense. The location of the eigenfrequencies are matched as well as the damping behavior. Also the distribution of the dofs over the thickness are approximated very well. Incorporating additional quantities from the series expansions is straightforward. Still, a general truncation strategy cannot be given easily, since this may vary from problem to problem. Of course, the thickness of the plate is

the main property influencing the need of higher order terms. Moreover, it can be stated that the terms of higher order are especially required for matching a realistic behavior in the neighborhood of edges and clamps. It should also be mentioned that the presented formulation is not restricted to plate problems. The in-plane problem can be treated in the same manner.

A specific value for the speedup in computation time compared to the 3d system can not easily be given since too many factors play a role in it. A higher resolution of the discretization over the thickness slows down the 3d calculation extremely, whereas the same discretization over the plane may not be needed at all to obtain similar results. In addition, both implementations are far from being optimized. However, to give an idea, on a single local machine, the plate computation for figure 3 was done during a short coffee-brake, whereas solving the 3d system took up most of the night.

Since the main goal of the present work is to show the fundamental functionality of the proposed system, it is renounced on a more sophisticated and optimized finite element formulation. The use of mixed methods and non-conforming finite element spaces is common practice when it comes to the numerical solution of the classical plate equations [7]. The use of such practices and their effects on the plate formulation given here has still to be elaborated.

A common effect observed in conjunction with the finite element solution of shear-deformable plates is the so-called shear-locking. It mainly arises when using conforming elements of low polynom order on thin structures, i.e., if $h \to 0$. Its impact on the presented formulation has not yet been investigated.

Obviously, it should always be kept in mind that a plate represents just an approximation of the full 3d system which, sooner or later, necessarily leads to some sort of mismatch. The reasons could be the use of inappropriate geometrical configurations as well as many possible issues arising from the numerical solution. All in all, in view of all calculations performed within the preparation of this article, the proposed formulation seems to represent an efficient alternative to the full 3d model and, hence, encourages to incorporate it into the elaboration of sound mitigation problems using poroelastic plate structures.

Acknowledgements The authors gratefully acknowledge the financial support by the Austrian Science Fund (FWF) under grant P-20420 as well as the fruitful and helpful discussions with R. Kienzler during their visits at the University of Bremen.

A Evaluated resultants

The procedure of evaluating the resultants is illustrated below on the example of the resultant $S_{\alpha\beta}$ where S_{11}, S_{22} are the bending moments and S_{12}, S_{21} are the twisting moments around the axes spanning the plane. Due to the symmetry of $\sigma_{\alpha\beta}$, the resultants $S_{\alpha\beta}$ are symmetric as well. This time, the order of the quantities resulting from the series expansions is denoted by the letter k in order to distinguish between the series used for the functions u_i and p and the series used for $\bar{u}_i$ and $\bar{p}$.

$$\begin{aligned}
\overset{\ell}{S}_{\alpha\beta} &= \int_h \sigma_{\alpha\beta} x_3^\ell \,\mathrm{d}x_3 = \int_h \left[\mu(u_{\alpha,\beta} + u_{\beta,\alpha}) + (\lambda u_{k,k} - \alpha p)\delta_{\alpha\beta}\right] x_3^\ell \,\mathrm{d}x_3 \\
&\approx \sum_{k=0}^{m} \int_h \left[\mu(\overset{k}{u}_{\alpha,\beta} + \overset{k}{u}_{\beta,\alpha}) + (\lambda \overset{k}{u}_{\gamma,\gamma} - \alpha \overset{k}{p})\delta_{\alpha\beta}\right] x_3^{(k+\ell)} \,\mathrm{d}x_3 + \sum_{k=0}^{n} \int_h \left[k\lambda \overset{k}{u}_3\right] x_3^{k+\ell-1} \,\mathrm{d}x_3 \\
&= \sum_{k=0}^{m} \left(\frac{h}{2}\right)^{k+\ell} \left[\delta^e_{kl} \frac{h}{k+\ell+1} \left[\mu(\overset{k}{u}_{\alpha,\beta} + \overset{k}{u}_{\beta,\alpha}) + (\lambda \overset{k}{u}_{\gamma,\gamma} - \alpha \overset{k}{p})\delta_{\alpha\beta}\right] + \delta^o_{kl} \frac{2k}{k+\ell} \left[\lambda \overset{k}{u}_3\right]\right]
\end{aligned} \tag{33}$$

with

$$\delta^e_{kl} = \frac{1+(-1)^{k+\ell}}{2} = \begin{cases} 1 & \text{if } k+\ell \text{ even} \\ 0 & \text{if } k+\ell \text{ odd} \end{cases} \qquad \delta^o_{kl} = \frac{1-(-1)^{k+\ell}}{2} = \begin{cases} 0 & \text{if } k+\ell \text{ even} \\ 1 & \text{if } k+\ell \text{ odd} \end{cases} .$$

Expression (33) is exemplary evaluated up to the order of 4, hence all terms of order $\mathcal{O}(5)$ and higher are neglected. Only the plate quantities are considered. The so-called plate parameter $c^2 = \frac{h^2}{12}$ is introduced. All even orders of $\overset{\ell}{S}_{\alpha\beta}$ turn out to be equal to zero, whereas the odd orders yield

$$\begin{aligned}
\overset{1}{S}_{\alpha\beta} &= \mu h \left[c^2 \left[\overset{1}{u}_{\alpha,\beta} + \overset{1}{u}_{\beta,\alpha} + \left(\frac{\lambda}{\mu} \overset{1}{u}_{\gamma,\gamma} - \frac{\alpha}{\mu} \overset{1}{p} + 2\frac{\lambda}{\mu} \overset{2}{u}_3\right)\delta_{\alpha\beta}\right]\right. \\
&\quad \left. + \frac{9}{5} c^4 \left[\overset{3}{u}_{\alpha,\beta} + \overset{3}{u}_{\beta,\alpha} + \left(\frac{\lambda}{\mu} \overset{3}{u}_{\gamma,\gamma} - \frac{\alpha}{\mu} \overset{3}{p} + 4\frac{\lambda}{\mu} \overset{4}{u}_3\right)\delta_{\alpha\beta}\right] + \mathcal{O}(5)\right] \\
\overset{3}{S}_{\alpha\beta} &= \mu h \left[\frac{9}{5} c^4 \left[\overset{1}{u}_{\alpha,\beta} + \overset{1}{u}_{\beta,\alpha} + \left(\frac{\lambda}{\mu} \overset{1}{u}_{\gamma,\gamma} - \frac{\alpha}{\mu} \overset{1}{p} + 2\frac{\lambda}{\mu} \overset{2}{u}_3\right)\delta_{\alpha\beta}\right]\right. \\
&\quad \left. + \frac{27}{7} c^6 \left[\overset{3}{u}_{\alpha,\beta} + \overset{3}{u}_{\beta,\alpha} + \left(\frac{\lambda}{\mu} \overset{3}{u}_{\gamma,\gamma} - \frac{\alpha}{\mu} \overset{3}{p} + 4\frac{\lambda}{\mu} \overset{4}{u}_3\right)\delta_{\alpha\beta}\right] + \mathcal{O}(5)\right] \\
\overset{5}{S}_{\alpha\beta} &= \mathcal{O}(5)
\end{aligned} \tag{34}$$

The same procedure has to be applied on all resultants. The final expressions are given below.

Shear forces $\overset{\ell}{S}_{\alpha 3} = \overset{\ell}{S}_{3\alpha}$ with $\ell \in \mathbb{E}$

$$\begin{aligned}
\overset{0}{S}_{3\alpha} &= \mu h \left[\overset{0}{u}_{3,\alpha} + \overset{1}{u}_{\alpha} + c^2 \left(\overset{2}{u}_{3,\alpha} + 3\overset{3}{u}_{\alpha} \right) + \frac{9}{5} c^4 \overset{4}{u}_{3,\alpha} + \mathcal{O}(5) \right] \\
\overset{2}{S}_{3\alpha} &= \mu h \left[c^2 \left(\overset{0}{u}_{3,\alpha} + \overset{1}{u}_{\alpha} \right) + \frac{9}{5} c^4 \left(\overset{2}{u}_{3,\alpha} + 3\overset{3}{u}_{\alpha} \right) + \frac{27}{7} c^6 \overset{4}{u}_{3,\alpha} + \mathcal{O}(5) \right] \\
\overset{4}{S}_{3\alpha} &= \mu h \left[\frac{9}{5} c^4 \left(\overset{0}{u}_{3,\alpha} + \overset{1}{u}_{\alpha} \right) + \frac{27}{7} c^6 \left(\overset{2}{u}_{3,\alpha} + 3\overset{3}{u}_{\alpha} \right) + 9c^8 \overset{4}{u}_{3,\alpha} + \mathcal{O}(5) \right] \\
\overset{6}{S}_{3\alpha} &= \mathcal{O}(5)
\end{aligned} \tag{35}$$

Resultant $\overset{\ell}{S}_{33}$ with $\ell \in \mathbb{O}$

$$\begin{aligned}
\overset{1}{S}_{33} &= \mu h \left[c^2 \left[\frac{\lambda}{\mu} \overset{1}{u}_{\gamma,\gamma} - \frac{\alpha}{\mu} \overset{1}{p} + 2\frac{2\mu+\lambda}{\mu} \overset{2}{u}_3 \right] + \frac{9}{5} c^4 \left[\frac{\lambda}{\mu} \overset{3}{u}_{\gamma,\gamma} - \frac{\alpha}{\mu} \overset{3}{p} + 4\frac{2\mu+\lambda}{\mu} \overset{4}{u}_3 \right] + \mathcal{O}(5) \right] \\
\overset{3}{S}_{33} &= \mu h \left[\frac{9}{5} c^4 \left[\frac{\lambda}{\mu} \overset{1}{u}_{\gamma,\gamma} - \frac{\alpha}{\mu} \overset{1}{p} + 2\frac{2\mu+\lambda}{\mu} \overset{2}{u}_3 \right] + \frac{27}{7} c^6 \left[\frac{\lambda}{\mu} \overset{3}{u}_{\gamma,\gamma} - \frac{\alpha}{\mu} \overset{3}{p} + 4\frac{(2\mu+\lambda)}{\mu} \overset{4}{u}_3 \right] + \mathcal{O}(5) \right] \\
\overset{5}{S}_{33} &= \mathcal{O}(5)
\end{aligned} \tag{36}$$

Resultant $\overset{\ell}{Q}_{\alpha}$ with $\ell \in \mathbb{O}$

$$\begin{aligned}
\overset{1}{Q}_{\alpha} &= \mu h \, \mathrm{i}\omega \frac{\beta}{\mu} \left[c^2 \left[-\frac{1}{\omega^2 \rho_f} \overset{1}{p}_{,\alpha} + \overset{1}{u}_{\alpha} \right] + \frac{9}{5} c^4 \left[-\frac{1}{\omega^2 \rho_f} \overset{3}{p}_{,\alpha} + \overset{3}{u}_{\alpha} \right] + \mathcal{O}(5) \right] \\
\overset{3}{Q}_{\alpha} &= \mu h \, \mathrm{i}\omega \frac{\beta}{\mu} \left[\frac{9}{5} c^4 \left[-\frac{1}{\omega^2 \rho_f} \overset{1}{p}_{,\alpha} + \overset{1}{u}_{\alpha} \right] + \frac{27}{7} c^6 \left[-\frac{1}{\omega^2 \rho_f} \overset{3}{p}_{,\alpha} + \overset{3}{u}_{\alpha} \right] + \mathcal{O}(5) \right] \\
\overset{5}{Q}_{\alpha} &= \mathcal{O}(5)
\end{aligned} \tag{37}$$

Total out−of−plane flux $\overset{\ell}{Q}_3$ with $\ell \in \mathbb{E}$

$$\begin{aligned}
\overset{0}{Q}_3 &= \mu h \, \mathrm{i}\omega \frac{\beta}{\mu} \left[\left[\frac{1}{\omega^2 \rho_f} \left(-\overset{1}{p} + f_3^f \right) + \overset{0}{u}_3 \right] + c^2 \left[-3\frac{1}{\omega^2 \rho_f} \overset{3}{p} + \overset{2}{u}_3 \right] + \frac{9}{5} c^4 \overset{4}{u}_3 + \mathcal{O}(5) \right] \\
\overset{2}{Q}_3 &= \mu h \, \mathrm{i}\omega \frac{\beta}{\mu} \left[c^2 \left[\frac{1}{\omega^2 \rho_f} \left(-\overset{1}{p} + f_3^f \right) + \overset{0}{u}_3 \right] + \frac{9}{5} c^4 \left[-3\frac{1}{\omega^2 \rho_f} \overset{3}{p} + \overset{2}{u}_3 \right] + \frac{27}{7} c^6 \overset{4}{u}_3 + \mathcal{O}(5) \right] \\
\overset{4}{Q}_3 &= \mu h \, \mathrm{i}\omega \frac{\beta}{\mu} \left[\frac{9}{5} c^4 \left[\frac{1}{\omega^2 \rho_f} \left(-\overset{1}{p} + f_3^f \right) + \overset{0}{u}_3 \right] + \frac{27}{7} c^6 \left[-3\frac{1}{\omega^2 \rho_f} \overset{3}{p} + \overset{2}{u}_3 \right] + 9c^8 \overset{4}{u}_3 + \mathcal{O}(5) \right] \\
\overset{6}{Q}_3 &= \mathcal{O}(5)
\end{aligned} \tag{38}$$

Resultant $\overset{\ell}{T}_\alpha$ with $\ell \in \mathbb{O}$

$$\begin{aligned}
\overset{1}{T}_\alpha &= h\left[c^2\left[-\omega^2(\rho+\beta\rho^f)\overset{1}{u}_\alpha+\beta\overset{1}{p}_{,\alpha}\right]+\frac{9}{5}c^4\left[-\omega^2(\rho+\beta\rho^f)\overset{3}{u}_\alpha+\beta\overset{3}{p}_{,\alpha}\right]+\mathcal{O}(5)\right]\\
\overset{3}{T}_\alpha &= h\left[\frac{9}{5}c^4\left[-\omega^2(\rho+\beta\rho^f)\overset{1}{u}_\alpha+\beta\overset{1}{p}_{,\alpha}\right]+\frac{27}{7}c^6\left[-\omega^2(\rho+\beta\rho^f)\overset{3}{u}_\alpha+\beta\overset{3}{p}_{,\alpha}\right]+\mathcal{O}(5)\right]\\
\overset{5}{T}_\alpha &= \mathcal{O}(5)
\end{aligned} \tag{39}$$

Resultant $\overset{\ell}{T}_3$ with $\ell \in \mathbb{E}$

$$\begin{aligned}
\overset{0}{T}_3 &= h\left[\left[-\omega^2(\rho+\beta\rho^f)\overset{0}{u}_3-\beta f_3^f-f_3+\beta\overset{1}{p}\right]+c^2\left[-\omega^2(\rho+\beta\rho^f)\overset{2}{u}_3+3\beta\overset{3}{p}\right]\right.\\
&\quad\left.+\frac{9}{5}c^4\left[-\omega^2(\rho+\beta\rho^f)\overset{4}{u}_3\right]+\mathcal{O}(5)\right]\\
\overset{2}{T}_3 &= h\left[c^2\left[-\omega^2(\rho+\beta\rho^f)\overset{0}{u}_3-\beta f_3^f-f_3+\beta\overset{1}{p}\right]+\frac{9}{5}c^4\left[-\omega^2(\rho+\beta\rho^f)\overset{2}{u}_3+3\beta\overset{3}{p}\right]\right.\\
&\quad\left.+\frac{27}{7}c^6\left[-\omega^2(\rho+\beta\rho^f)\overset{4}{u}_3\right]+\mathcal{O}(5)\right]\\
\overset{4}{T}_3 &= h\left[\frac{9}{5}c^4\left[-\omega^2(\rho+\beta\rho^f)\overset{0}{u}_3-\beta f_3^f-f_3+\beta\overset{1}{p}\right]+\frac{27}{7}c^6\left[-\omega^2(\rho+\beta\rho^f)\overset{2}{u}_3+3\beta\overset{3}{p}\right]\right.\\
&\quad\left.+9c^8\left[-\omega^2(\rho+\beta\rho^f)\overset{4}{u}_3\right]+\mathcal{O}(5)\right]\\
\overset{6}{T}_3 &= \mathcal{O}(5)
\end{aligned} \tag{40}$$

Resultant $\overset{\ell}{P}$ with $\ell \in \mathbb{O}$

$$\begin{aligned}
\overset{1}{P} &= -hi\omega\left[c^2\left[\alpha\overset{1}{u}_{\gamma,\gamma}+\frac{\phi^2}{R}\overset{1}{p}+2\alpha\overset{2}{u}_3\right]+\frac{9}{5}c^4\left[\alpha\overset{3}{u}_{\gamma,\gamma}+\frac{\phi^2}{R}\overset{3}{p}+4\alpha\overset{4}{u}_3\right]+\mathcal{O}(5)\right]\\
\overset{3}{P} &= -hi\omega\left[\frac{9}{5}c^4\left[\alpha\overset{1}{u}_{\gamma,\gamma}+\frac{\phi^2}{R}\overset{1}{p}+2\alpha\overset{2}{u}_3\right]+\frac{27}{7}c^6\left[\alpha\overset{3}{u}_{\gamma,\gamma}+\frac{\phi^2}{R}\overset{3}{p}+4\alpha\overset{4}{u}_3\right]+\mathcal{O}(5)\right]\\
\overset{5}{P} &= \mathcal{O}(5)
\end{aligned} \tag{41}$$

References

[1] N. Atalla, R. Panneton, and P. Debergue. A mixed displacement-pressure formulation for poroelastic materials. *Journal of the Acoustical Society of America*, 104(3):1444–1452, 1998.

[2] M. A. Biot. General theory of three-dimensional consolidation. *Journal of Applied Physics*, 12:155–164, 1941.

[3] M. A. Biot. Theory of elasticity and consolidation for a porous anisotropic solid. *Journal of Applied Physics*, 26:182–185, 1955.

[4] M. A. Biot. Theory of propagation of elastic waves in a fluid-saturated porous solid.I/II. Lower/Higher frequency range. *Journal of the Acoustical Society of America*, 28(2):168–178, 1956.

[5] M. A. Biot. Theory of deformation of a porous viscoelastic anisotropic solid. *Journal of Applied Physics*, 27(5):459–467, 1956.

[6] G. Bonnet and J. L. Auriault. *Dynamics of Saturated and Deformable Porous Media: Homogenization Theory and Determination of the Solid-Liquid Coupling Coefficients*, pages 306–316. Physics of Finely Divided Matter. Springer Verlag, Berlin, 1985.

[7] D. Braess. *Finite Elemente*. Springer, 2007.

[8] G. Cederbaum, L. Li, and K. Schulgasser. *Poroelastic Structures*. Elsevier Science, 2000.

[9] E. Detournay and A. H. D. Cheng. *Fundamentals of Poroelasticity*, volume 2 of *Comprehensive Rock Engineering*, chapter 5, pages 113–171. Pergamon Press, Oxford, 1993.

[10] T. J. R. Hughes. *The Finite Element Method - Linear Static and Dynamic Finite Element Analysis*. Dover Publications Inc., 1987.

[11] D. Johnson, J. Koplik, and R. Dashen. Theory of dynamic permeability and tortuosity in fluid saturated porous media. *Journal of Fluid Mechanics*, 176:379–402, 1987.

[12] R. Kienzler. On consistent plate theories. *Archive of Applied Mechanics*, 72:229–247, 2002.

[13] R. Kienzler. On consistent second-order plate theories. In *Theories of Plates and Shells: Critical Review and New Applications (Lecture Notes in Applied and Computational Mechanics)*, volume 16, pages 85–96. Springer, 2004.

[14] B. Kirk, J. W. Peterson, R. H. Stogner, and G. F. Carey. `libMesh`: A C++ Library for Parallel Adaptive Mesh Refinement/Coarsening Simulations. *Engineering with Computers*, 22(3–4):237–254, 2006.

[15] P. Leclaire, K. V. Horoshenkov, and A. Cummings. Transverse vibrations of a thin rectangular porous plate saturated by a fluid. *Journal of Sound and Vibration*, 247(1):1–18, 2001.

[16] R. W. Lewis and B. A. Schrefler. *The Finite Element Method in the Static and Dynamic Deformation and Consolidation of Porous Media*. Wiley, 2 edition, 1998.

[17] R. D. Mindlin. *An Introduction to the Mathematical Theory of Vibration of Elastic Plates*. World Scientific Publishing Co. Pte. Ltd, 2006.

[18] G. Preußer. Eine systematische Herleitung verbesserter Plattengleichungen. *Archive of Applied Mechanics*, 54(1):51–61, 1984.

[19] M. Schanz and D. Pryl. Dynamic fundamental solutions for compressible and incompressible modeled poroelastic continua. *International Journal for Solids and Structures*, 41(15): 4047–4073, 2004.

[20] L. A. Taber. A theory for transverse deflection of poroelastic plates. *Journal of Applied Mechanics*, 59:628–634, 1992.

[21] D. D. Theodorakopoulos and D. E. Beskos. Flexural vibrations of poroelastic plates. *Acta Mechanica*, 103:191–203, 1994.

[22] K. Wilmanski. A few remarks on Biot's model and linear acoustics of poroelastic saturated material. *Soil Dynamics and Earthquake Engineering*, 26:509–536, 2006.